Metals & corrosion



Cold angular rolling process as a continuous severe plastic deformation technique

Leonardo M. Reis^{1,2}, Amanda P. Carvalho², Isshu Lee³, Yun-Hsuan Wu³, Jae-Kyung Han³, Melissa K. Santala³, Megumi Kawasaki^{3,*} , and Roberto B. Figueiredo^{2,*}

Received: 28 October 2022 Accepted: 7 February 2023 Published online: 24 February 2023

© The Author(s), under exclusive licence to Springer Science+Business Media, LLC, part of Springer Nature 2023

ABSTRACT

Cold angular rolling process (CARP) has emerged as a potential continuous severe plastic deformation technique enabling the processing of bulk metal sheets with improved mechanical properties. The CARP technique involves a combination of cold rolling of a sheet by a single rotation roller followed by equal-channel angular pressing of the sheet passing through a bent channel. The present work uses finite element method (FEM) to model CARP by considering processing conditions, including different friction values and processing velocities for different copper and stainless steel alloys. The simulations reveal the influence of these processing parameters on distributions of strain, strain rate, stress (in both the metal sheet and the CARP tool), temperature, and torque requirements through one pass of CARP on the metal sheets. The modeling results are validated by the experimental characterization of the hardness distribution and microstructure after CARP on a copper sheet. The results from FEM are used to estimate the energy incorporated into different metal alloys at various processing conditions. Finally, this study discusses the feasibility of scaling up the CARP technique.

Handling Editor: P. Nash.



¹ Department of Materials Engineering and Civil Construction, Universidade Federal de Minas Gerais, Belo Horizonte, MG 31270-901, Brazil

²Department of Metallurgical and Materials Engineering, Universidade Federal de Minas Gerais, Belo Horizonte, MG 31270-901, Brazil

³ School of Mechanical, Industrial and Manufacturing Engineering, Oregon State University, Corvallis, OR 97331, USA

Hardness

Cold Angular Rolling Process (CARP) Experiments Microstructure

Temperature rise

Copper Friction: 0.10

FEM simulation

Plastic strain

Copper Friction: 0.10

Velocity: ~5 mm/s

GRAPHICAL ABSTRACT

Introduction

Metal manufacturing industry has been searching for the processing routes enabling the refinement of grain structure in bulk metallic materials for improving mechanical properties. The available routes for reducing grain size include the use of alloying elements during solidification of melts and the controlled recrystallization mechanisms of metals through thermo-mechanical processes. Processing of engineering metals and materials by severe plastic deformation gained significant attention in the last three decades [1, 2] due to the ability to produce bulk metal samples with ultrafine grain sizes ($< 1 \mu m$) which cannot be obtained through the conventional processing operations [3]. Severe plastic deformation generally leads to a significant improvement in strength [4] and superplastic ductilities even at ambient temperatures [5]. Efforts have been made to adapt these techniques to a continuous manufacturing process, so that high-strength sheet metals can be produced in an economically-viable industrial processing route.

Earlier reports demonstrated that it is feasible to adapt a component of equal-channel angular pressing (ECAP) [6] to continuous processing through the use of the Conform concept [7]. The approach was initially developed to enable continuous extrusion of metals, but its principles can be used in the ECAP

procedure and has been applied to process wires and thin rods of commercial purity Al [8], Al-6061 [9], and commercial purity Ti [10]. In fact, ECAP-Conform is already used in commercialization of nanostructured metals in shapes of wires and rods [11]. Despite the success in the use of the principle of Conform to produce metal bars, rods, and wires, the continuous process of sheet metals remains a technological challenge. It is feasible to modify and adapt a pair of rolling mills through intersecting channels, thereby imposing shear deformation on metallic sheets. This process is called equal-channel angular rolling (ECAR) and it has been applied to aluminum alloys of Al-1100 [12], Al-6063 [13], Al-5052 and Al-7057 [14], an AZ 31 magnesium alloy [15], and a commercial purity Cu [16]. In addition, a process called continuous frictional angular extrusion has been applied to commercial purity Al [17].

Another approach to achieve grain refinement in a continuous process—which is pursued here—is to drive a metallic sheet by a single roller, which is enclosed by a circumferential die followed by a bent channel for a sheet to experience an ECAP-like shear deformation. The process engages circumferential shear deformation under compression followed by the channel-angle deformation, enabling the singlestep, continuous process of metallic sheets. The present processing procedure is similar to ECAP-Conform, except that continuous sheet-metal processing is possible with CARP. The concept of the cold



angular rolling process (CARP) was first introduced as single-roll angular-rolling (SRAR) [18] and the refined microstructure and improved mechanical properties has been studied in conjunction with the processing operations of numbers of passes [19], additional annealing after processing [20], different processing routes as seen in ECAP [21] and additional surface treatment after processing [22]. The CARP technique improves the rolling segment by additional reduction in sheet thickness for severe plastic deformation. The present work provides evaluation through simulation and experiments to investigate the processing capability for bulk metal sheets.

Finite element method (FEM) is a powerful tool to study severe plastic deformation techniques, especially when considering various samples and processing conditions [23] and complex processing that combines two or more separate processing techniques [24, 25]. FEM has often applied to the mechanics of ECAP [26]. For example, FEM simulation can help predict and understand the effects of the corner gap [27–29], processing temperature [30], stress distribution, damage accumulation [31–34], development of plastic instabilities [35, 36] and backpressure [36, 37] on the heterogeneous deformation. FEM has been used to model continuous ECAP process operations including continuous confined strip shearing [38, 39] and ECAP-conform [40] where the techniques are similar each other, equal-channel angular rolling [41], as well as SRAR [18, 19, 21], where the focus has been limited to the estimation of the effective deformation distribution in the processed sheets. To meet the demand for scaling up of metal processing, it is important to understand the distributions of strain, stresses (mean and effective), and temperature within the sheets for the significance of plastic deformation by the CARP technique. In addition, it is essential to determine the influence of friction factor and processing velocity on a required strength and torque of the CARP tools for the continuous sheet metal process. The present work uses FEM to improve the understanding of the CARP technique. Moreover, initial experimental results from CARP-processed Cu sheets are compared with the FEM results. This study provides a framework to tailor desirable characteristics in the produced metal sheets and for the scale-up of continuous metal processing techniques.

Experimental procedures

Sheet processing by CARP

The fundamentals of CARP are similar to those for SRAR [18], where the rotational roll and stationary circumferential die as shown in Fig. 1a is attached on the rotational stage of high-pressure torsion (HPT) facility. The stationary die has an entrance for a sheet metal with a thickness of 1.0 mm, and it is rolled under compression to reduce the thickness gradually to 0.9 mm before it enters a bent channel with a channel angle of 135° which introduced ECAP-like processing. After the bent channel, the die provides a space of 1.0 mm thickness for a sheet metal. A schematic die configuration at compressive cold rolling followed by channel-angle processing is shown in Fig. 1b. The operation of CARP using a commercial purity (CP) Cu (< 99.5% pure) plate is shown in Fig. 1d, where the rotating roller pushes the sheet through the die, reducing its thickness reduction as forcing it into the channel-angle at a selected processing speed, i.e., 1.0 rotation per minute (rpm) of the rotating roll. Cu sheets are shown in Fig. 1c before processing (bottom), a sheet runs two-thirds of its length processed by CARP, and a fully CARPprocessed sheet. This commercial purity Cu sheet having 3.5 cm width $\times 35 \text{ cm}$ length $\times 0.1 \text{ cm}$ thickness was processed by CARP at room temperature for 1 pass at a processing speed of 5 mm/sec by applying an HPT anvil rotation at 1 rpm. The sheets were acquired and processed from the as-rolled condition. The initial Vickers microhardness of the as-rolled sheet was $H_V = 91 \pm 3$. Note: There is no limitation in the length of sheets for processing by CARP, even though the experiments used sheet metals of a specific length. Oil-base lubricant (WD40 ®) was applied to one side of the copper sheet surfaces to minimize friction between the sheet and stationary die.

Finite element modeling

A commercial finite element analysis software QForm (version 10.1.3) [42] was used in the present work. The simulations considered 2D plane strain conditions with thermal effects and elastic–plastic deformation. The mesh was composed of triangular elements with the maximum edge length of 0.5 mm. A refined mesh, with the maximum edge length of



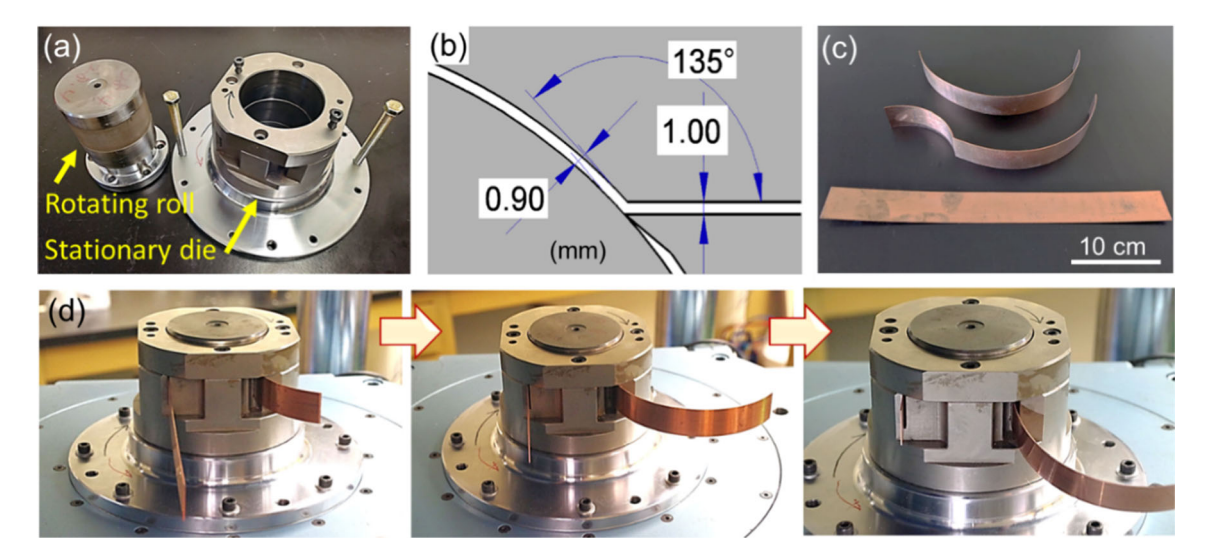


Figure 1 a the CARP accessory with the rotating roll removed from its die, **b** the die configuration at the point where it transitions to the channel angle of 135°, **c** a Cu sheet before processing

(bottom), a sheet removed from the die during processing (middle), and a complete CARP-processed sheet (top), and **d** photos showing processing of a Cu sheet by CARP.

0.2 mm, was adopted in the shearing deformation region. The total number of elements was ~ 2500 and this mesh size was found to reproduce local heterogeneities in deformation distribution. Automatic remeshing was set at every 20 steps and the

step size was either a maximum strain of 0.1 or 0.5 s. The computer-modeled CARP processing tool is shown in Fig. 2a. The dimension and constraints of CARP for FEM follow the actual CARP design as was shown in Fig. 1b. Friction between the work piece

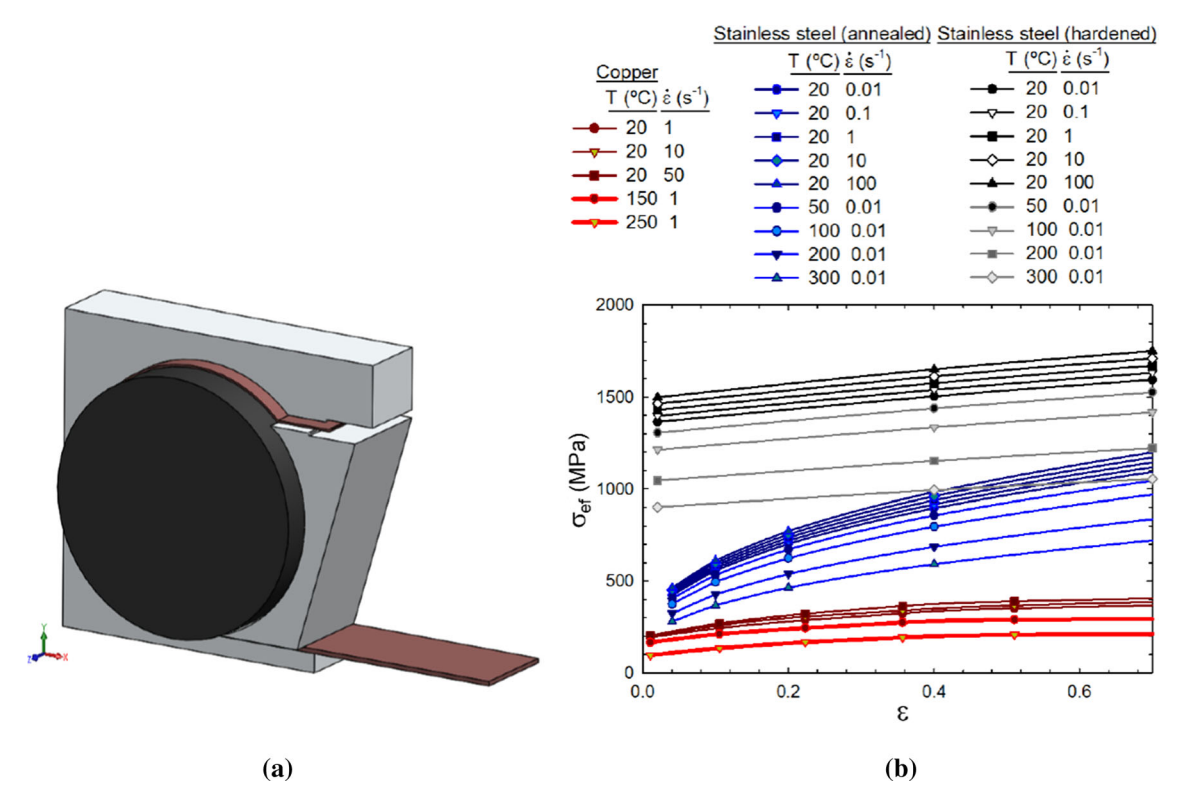


Figure 2 a Illustration of the FEM model of CARP operation and b stress vs strain curves for the different material conditions considered in the simulations.



and the tools, τ , was computed by considering Levanov friction law [43]:

$$\tau = m \frac{\sigma_s}{\sqrt{3}} \left(1 - e^{-b\frac{\sigma_n}{\sigma_s}} \right) \tag{1}$$

where m is a friction factor, b is a constant equal to 1.25, σ_n is the contact pressure, and σ_s is the material's flow stress. This friction model was used because it considers the effect of contact pressure on friction stress, while it is limited to a maximum value of friction stress. Simulations were carried out by considering a frictionless condition with a friction factor, m, of 0.0, an intermediate condition with m = 0.05, and a condition for lubricated cold forming of copper alloys with m = 0.10. The coefficient of thermal transfer between the work piece and the tools was set to 90 kW/m² K. The simulations of the CARP deformation are considered for two different materials: copper and a stainless steel. Copper is largely used as a model material in finite element simulations, while stainless steel is applied to consider the feasibility of the process for common metals having high strength and broad commercial application. The CARP tool and metal sheet properties used in the simulations were based on data from the QForm software library and are summarized in Table 1. The properties of the stainless steel used in this study is based on an X5CrNi 18-10 stainless steel alloy.

The plastic behavior of the metal sheets was modeled by considering different stress versus strain $(\sigma \text{ vs. } \varepsilon)$ relationships at various temperatures and strain rates, which were obtained from the software library. The behavior of the stainless steel (SS) was modeled in two conditions: as-annealed and strain hardened. The latter condition aims to evaluate CARP processing of the material showing high flow stresses. The simulated values of the σ versus ε curves are shown in Fig. 2b. The simulations of CARP processing on copper uses three different rotation rates of the rotating roll of 1, 3 and 10 rpm to evaluate the effect of processing velocity on the distribution stress and strain of the sheet. These rotation rates produce of $\sim 5 \text{ mm/s}$, $\sim 16 \text{ mm/s}$ velocities

Table 1 Summary of the values of thermal conductivity K, coefficient of thermal expansion α , specific heat c, elastic modulus E, Poisson

	K (W m ⁻¹ K ⁻¹)	$\alpha (\times 10^5) (K^{-1})$	$c (J kg^{-1} K^{-1})$	E (GPa)	ν	$\rho \text{ (kg m}^{-3}\text{)}$
Copper	385	1.61	390	125	0.35	8890
Stainless steel	37.7	1.12	499	218	0.3	7850
CARP tool	21.3	-	460	200	0.3	8160

mm/s of the sheet. In addition, simulations were carried out with three different friction factors to evaluate the influence of the parameter on the modeling results.

Hardness and microstructure measurements

A Cu sheet was removed from the die when over half of the sheet was processed by CARP, while the remaining portion was under compression by rolling before experiencing shear deformation by ECAP as is shown in middle in Fig. 1c. Cross-sections along the rolling direction (RD) and normal direction (ND) were examined for the hardness distribution by Vickers microhardness and the microstructure after CARP by optical microscopy (OM) and electron backscatter diffraction (EBSD). All samples were stored at < 275 K after processing and between the sample preparation steps in order to prevent significant self-recovery of Cu that has been reported after ECAP [44] and HPT [44–46].

A section of the Cu sheet after CARP was mounted to reveal the cross-section and mechanically polished for the Vickers microhardness measurements using a Mitutoyo HM-200 with a load of 50 gf. The hardness values were measured with applying a rectilinear grid pattern with 0.15 mm separation between the adjacent points. The hardness values are utilized to generate a color-coded contour hardness map for the examined cross-section. Some regions of interest were examined by OM. The polished surface was chemically etched with a solution of HCl 25 ml, FeCl₃ 8 g, and H₂O 100 ml. Another specimen was cold mounted with the conductive carbon powder and castable acrylic mount. It was mechanically polished to have a mirror-like finish using 0.05 µm silica suspension for the final polishing step. The EBSD was conducted using a Quanta 3D Dual Beam scanning electron microscopy (SEM). The acceleration voltage and the working distance were 15 kV and 12 mm, respectively. The step size was set as 0.24 µm. The data were analyzed using an EDAX orientation

imaging microscopy (OIM) system equipped with the SEM.

Results

FEM results for copper

Figure 3 shows the FEM-calculated distribution of plastic strain, ε , in the plastically deformed region of rolling followed by the channel angle in a Cu sheet during CARP at different friction factors and processing velocities. After a complete process of CARP for 1 pass, plastic strain of ~ 0.6 is introduced at the mid-thickness to the outer surfaces of the Cu sheets at all processing conditions, while slightly lower strain of 0.4-0.5 is computed close to the inner sheet surfaces. This heterogeneous strain distribution is often observed during ECAP processing, where the corner gap in the shear zone allows bending at the bottom of the sheet material instead of imposing simple shear [28, 29]. Such heterogeneous plastic deformation is also consistent with the reported simulation results for the SRAR process [18, 21], even though that procedure yields a thicker sample thickness of 0.96 mm during rolling than the current process of CARP which yields a thickness of 0.90 mm. Nevertheless, the increased plastic strain of > 0.4 is reasonable after shear deformation from the angle channel when considering the theoretical estimation of equivalent

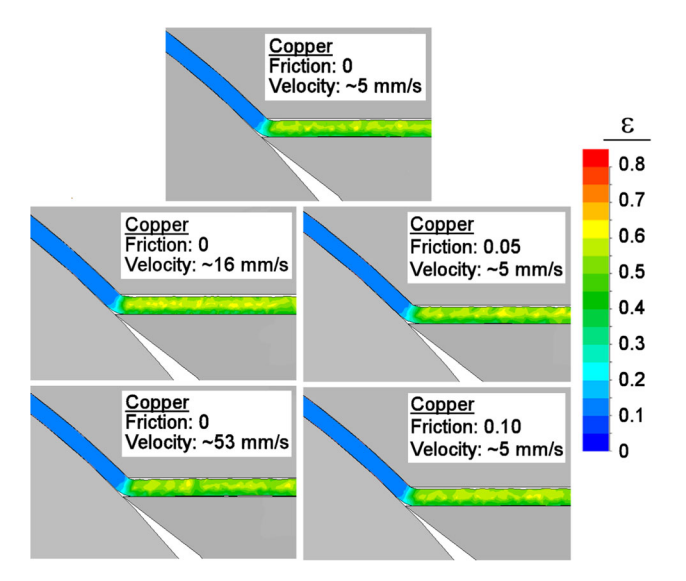


Figure 3 Distributions of plastic strain ε in a copper sheet during CARP with different processing velocities and friction factors from the FEM simulations.

plastic strain at the internal channel angle of 135° [47]. It should be noted that the friction factor and processing velocity do not influence the plastic strain.

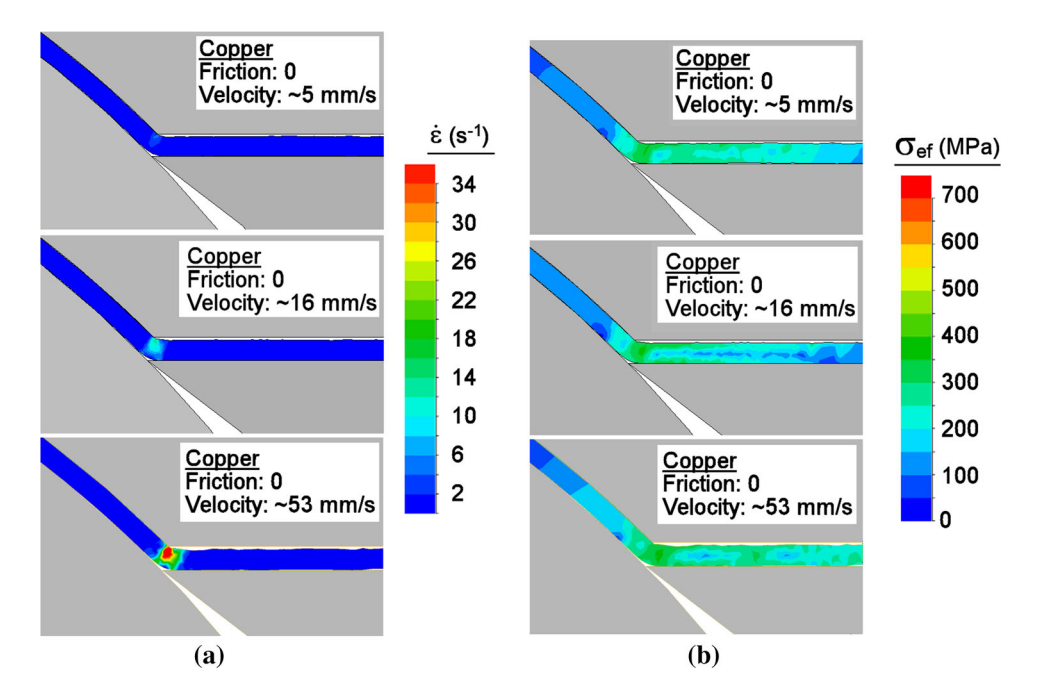
Figure 4a shows the distributions of strain rate, $\dot{\varepsilon}$, simulated at different processing velocities at the same deformation zone captured in Fig. 3 for the CARP operation. There is an increase in strain rate at the bent channel region with increased processing velocity. The change in strain rate slightly affects the stress required to process the Cu sheet material. Figure 4b shows the distributions of effective stress, $\sigma_{\rm ef}$, in the Cu sheet at different processing velocities. The effective stress was calculated considering the Von Mises criterion. The effective stress increases before the Cu sample reaches the channel-angle and the stress is the highest at the bent channel region. High stress is required when increasing the CARP processing velocity. Although the results are not shown, no significant change was observed in the present simulation in the distributions of strain rate and effective stresses with different friction factors of m = 0 to 0.1.

Figure 5 shows the distributions of mean stress, $\overline{\sigma}$, in the copper sheets through the entire CARP operation simulated with different friction factors and processing velocities. High compressive mean stresses are observed in the region where the sheet thickness is gradually reduced from 1.0 mm to 0.9 mm. With the thickness reduction, an increase in sheet length is required, causing a friction force on the sheet with both the rotating roll and the stationary die. Consequently, large compressive stresses develop within the Cu sheet, and the compressive mean stress is developed further with increasing processing velocity, which is attributed to the increased strength of the copper sheet at the increased deformation rates. The friction factor has an even more profound effect, so that an increase in friction factor introduces a pronounced increase in the mean compressive stresses at the shear deformation zone cause by rolling in CARP. Overall, all processing conditions modeled introduced the mean compressive stresses of at least ~ 0.8 GPa and the highest value of ~ 2 GPa developed within the thickness reduction zone during rolling in CARP for the highest friction modeled.

The distributions of temperature, T, in Cu sheets during CARP are shown in Fig. 6 for different simulated processing velocities (left column) and friction conditions (right column). At the end of the thickness



Figure 4 Distributions of a strain rate $\dot{\epsilon}$ and b effective stress $\sigma_{\rm ef}$ in a copper sheet during CARP with different processing velocities from the FEM simulations.



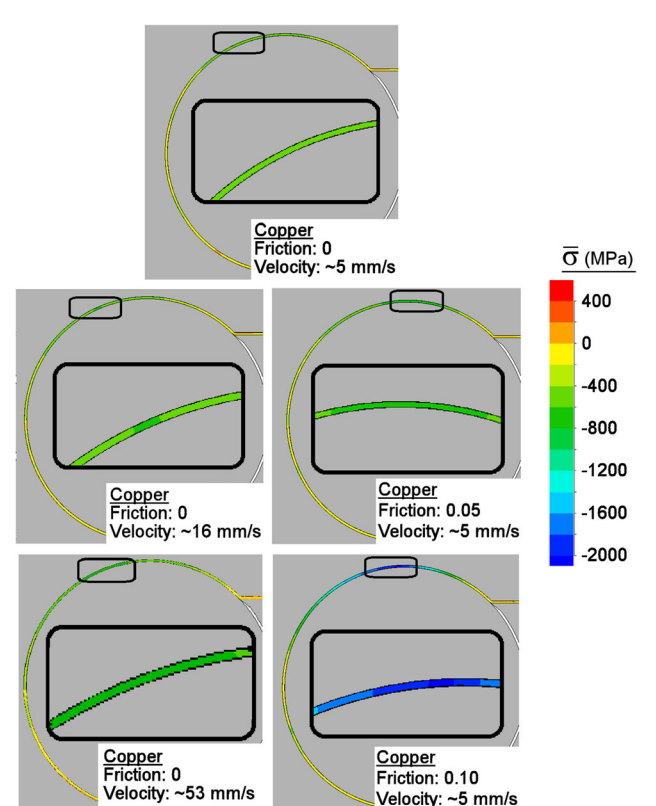


Figure 5 Distributions of mean stress $\overline{\sigma}$ in a copper sheet during CARP with different velocities and friction factors. The insets show the region of maximum stress for each processing condition.

reduction zone where high compressive mean stress develops (as seen in Fig. 5), only a slight increase in

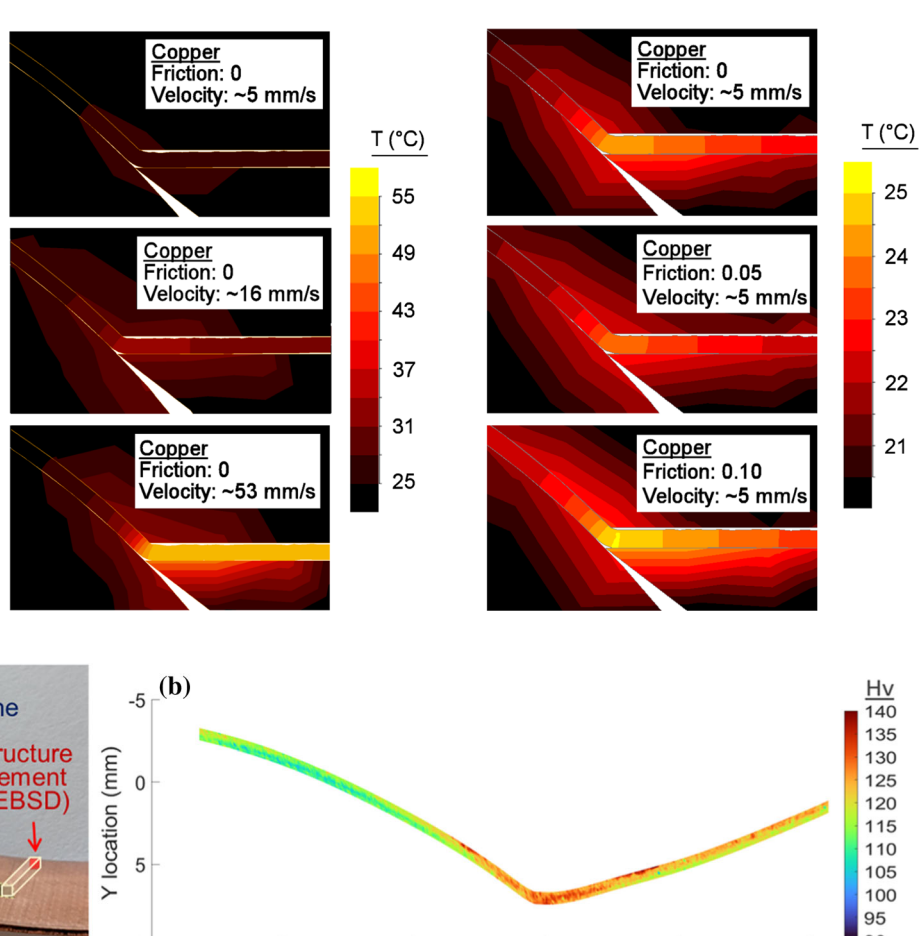
temperature of a few degrees Celsius, is calculated in the copper sheet. The temperature increases with increasing friction stresses, as seen in the right column of Fig. 6. The increase in friction factor increases the temperature of the copper sheet slightly before it reaches the ECAP shear deformation zone. The maximum temperature is observed in the region where plastic deformation occurs through the channel-angle component. Moreover, the processing velocity plays a major role in raising the sheet temperature at the shear deformation zone. The faster the processing speeds the faster the plastic deformation is imposed, reducing the time for heat conduction along the sheet. This factor contributes to the local increase in temperature. A temperature increase of ~ 30 °C is observed during CARP at the fastest processing velocity.

Experimental results for copper

A processing of a Cu sheet through CARP was performed to provide experimental validation of the FEM results. The sheet was processed at room temperature at a speed of 5 mm/s. Figure 7 shows (a) the sheet with annotations of the planes for the hardness and microstructural characterization, (b) a color-coded hardness contour map with the hardness scale, (c) OM micrographs taken at three different locations – shown in (a), and (d) an OIM image with a unit triangle of crystallographic orientation. The hardness



Figure 6 Distributions of temperature T in a copper sheet during the CARP operation simulated at various processing velocities and friction factors.



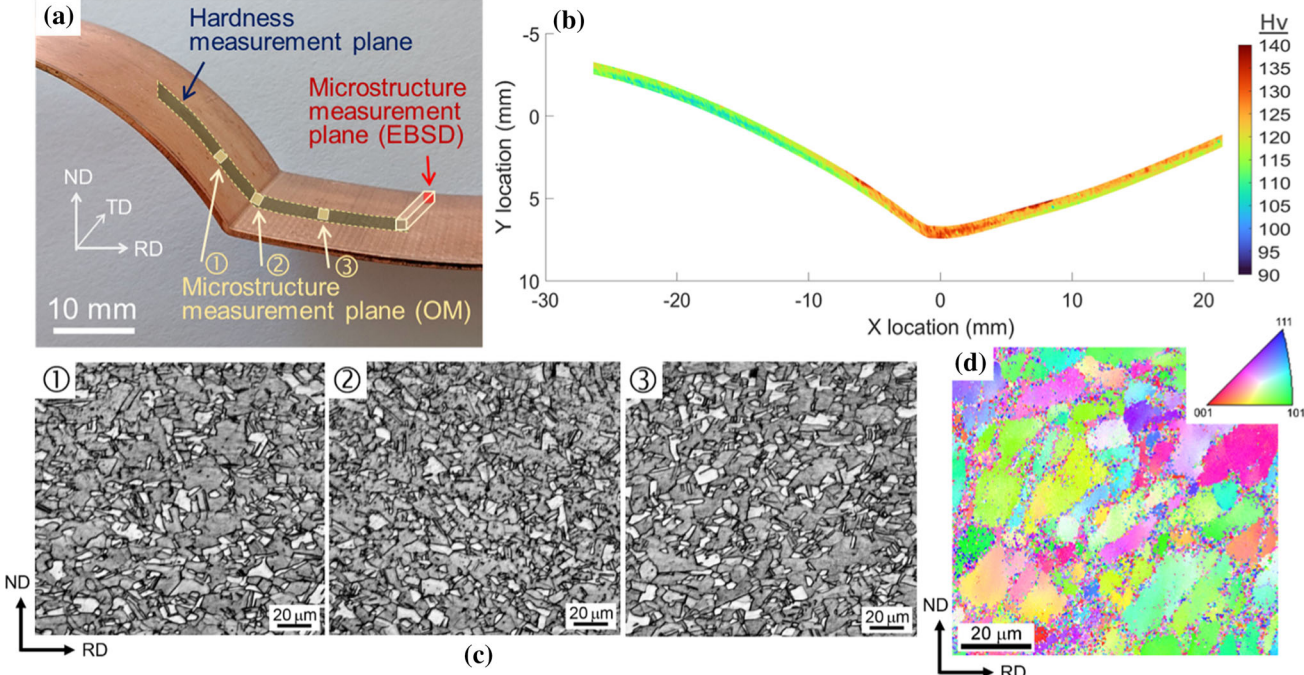


Figure 7 a a CARP-processed Cu sheet with the hardness and microstructural characterization locations, **b** a color-coded hardness contour map from the hardness measurement plane

shown in (a), c OM micrographs taken at the locations – shown in (a), and d an OIM image taken from the microstructure measurement plane shown in (a).

and OM micrographs were examined at the midwidth and the microstructure by EBSD was observed close to the edge of the cross-sections along the rolling direction (RD) and normal direction (ND) of the sheet.

The Cu sheet before CARP had an elongated grain morphology having longer and shorter grain

diameters of 20–30 μm and 5–10 μm , respectively, and the initial Vickers microhardness H_V was $\sim 91.$ The hardness increased up to ~ 130 immediately after the channel-angle shear zone and the recorded average value was 115 \pm 2 at the cross-section normal to the rolling direction. This maximum hardness value agrees with the reported value for the



commercial purity copper processed by ECAP for 1 pass at room temperature [48]. Slightly higher hardness is visible close to the outer surface of the sheet facing to the stationary die and it is consistent with the present FEM results, where high plastic strain presents close to the outer sheet surface, regardless of the friction factor, as shown in Fig. 3. There was a limited increase in hardness at the compression zone under rolling before the shear deformation zone at the channel-angle corner, while the required high torque to drive the copper sheet forward during the CARP operation confirmed the existence of significant compression stress at the compression zone as modeled in Fig. 5. The OM micrographs taken at the locations - suggests no significant changes in grain size and morphologies in the Cu sheet before, during, and after passing the channel-angle corner. The OIM image shows the slightly elongated grains aligning the channel-angle shear plane reasonably [47, 49]. The sub-grain morphology after CARP shows an average spatial sub-grain size of 7.6 \pm 2.8 microns.

A summary of the reported hardness changes and final grain sizes of pure copper processed by different continuous SPD processes including CARP is shown in Table 2. The hardness after one pass of CARP agrees with the values reported after 1 pass of other ECAP-based techniques, which tends to introduce a few tens of micron grain sizes in copper after a single process. The values of hardness reported in copper processed by continuous HPT techniques are higher

and the difference is attributed to the larger amount of strain imposed during HPT.

FEM results for stainless steel

FEM analysis was applied to examine the feasibility of CARP on other engineering metals. Figure 8 shows the FEM results describing the distributions of (a) effective plastic strain, ε , (b) strain rate, $\dot{\varepsilon}$, (c) effective stress, σ_{ef} , (d) simulated temperature, T, during CARP, and (e) mean stress $\overline{\sigma}$ of stainless steel (SS) at a velocity of ~ 53 mm/s with a friction factor of 0.05. Two conditions are considered in the simulations: an annealed sample and a strain-hardened sample. The distribution of strain in Fig. 8a shows that the annealed SS displays a similar pattern as was obtained for the copper in Fig. 3 showing high plastic strain close to the outer sheet surface. By contrast, it tends to be homogeneous along the sheet thickness of the hardened SS with some minor heterogeneities along the length of the sheet. This homogeneous strain distribution is attributed to a change in the distributions of strain rate in the deformation zone as shown in Fig. 8b, where the hardened SS is more resistant to additional strain hardening, which inhibits an influence of the corner gap that is known for reducing strain homogeneity [28, 54, 55]. Consequently, the deformation zone expands and shows relatively homogeneous deformation with its strain rate through the thickness of the sheet. In terms of the

Table 2 Summary of the hardness change and final grain size obtained in pure copper using different continuous SPD processes

Material	SPD process	No. of process	$\begin{array}{c} \text{Initial} \\ \text{hardness} \\ (H_V) \end{array}$	Final hardness $(H_{\rm V})$	Grian size after processing	Reference
CP-Cu (< 99.5%)	Cold angular rolling processing	1 pass	91 ± 3	115 ± 2	$7.6\pm2.8~\mu m$	This work
CP-Cu	Equal-channel angular rolling	1 pass	60	70 (center)/84 (surface)	\sim 14 \pm 9 μm	[16]
CP-Cu (99.99%)	Single-roll angular rolling	1 pass	50	110 ± 10	45.9 μm	[18]
Cu (99.5%)	ECAP-conform	1 pass	50 ± 1	110 ± 2	$5\pm1~\mu m$	[50]
Cu (99.9%)	Incremental high-pressure torsion	Single process (includes 15 HPT turns)	45	~ 120–140	Ultrafine grain size	[51]
Cu (99.99%)	Continuous high-pressure torsion	Single process	~ 80	130 (middle) / 133 (surface)	Submicron size	[52]
Cu (99.999%)	Continuous high-pressure torsion with wires	Single process	82	~ 126	0.3–0.4 μm	[53]



Stainless steel

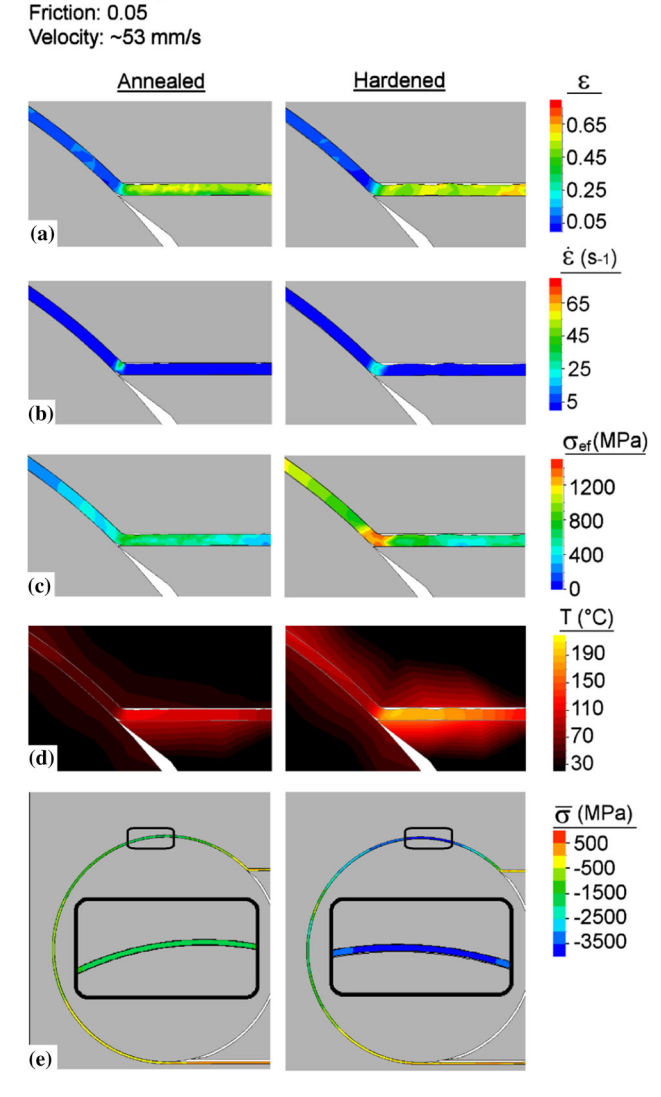


Figure 8 Distributions of **a** effective plastic strain ε , **b** strain rate $\dot{\varepsilon}$, **c** effective stress $\sigma_{\rm ef}$, **d** temperature T, and **e** mean stress $\overline{\sigma}$ during CARP of stainless steel sheets in the annealed and strainhardened conditions. The insets in **d** show details of the regions of highest mean stress.

effective stress, it is reasonable that the strain-hardened SS shows the higher values than in the annealed counterpart.

It is worth noting that the effective stresses of SS during CARP at room temperature as shown in Fig. 8c are slightly lower than the values in the stress–strain curves used in the current simulation (Fig. 2b). It is anticipated the heat generated during CARP leads to a decrease in the flow stress required for the deformation of SS. The simulated temperature distributions in the SS sheets and the surrounding tools are shown in Fig. 8d. It is apparent that there is

significant heating during processing. The initial temperature for both the sheet and the tools was set at 20 °C, and it increases to ~ 100 °C and ~ 200 °C for the annealed and the hardened SS, respectively, immediately after shear deformation at the ECAP corner. The general trend in the development of compressive mean stress as shown in Fig. 8e is consistent with the one described for the copper sheets in Fig. 5, while the computed values of the compressive stress are entirely high for the SS sheets. Compressive mean stresses of over 1.5 and 3 GPa develop in the annealed and hardened SS, respectively, within the thickness reduction zone during rolling. Such high stresses are anticipated to affect its frictional contact with the tool and thus the stress level of the tools.

Stress in the CARP tools

Considering the findings in the previous section, it is essential to understand how much the processing technique creates stresses on the processing dies. Figure 9 shows the distributions of effective stress in the CARP dies during processing of a copper at 5 mm/s with different friction factors and a hardened SS at the same processing velocity and friction used in Fig. 8. Higher stresses are observed in the rotating roll than the stationary die, and the stress value depends on the friction factor and the materials being processed. Specifically, the stress in the rotation

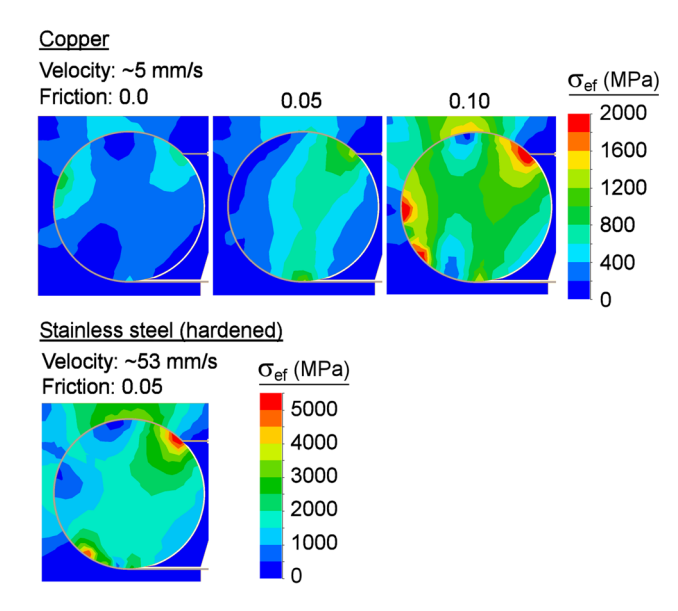


Figure 9 Distributions of effective stress $\sigma_{\rm ef}$ in the CARP tools during processing of copper at 5 mm/s with different friction factors and a hardened SS at 53 mm/s and a friction factor of 0.05.



roll increases from a maximum of ~ 1 GPa to a maximum of ~ 2 GPa with increasing the friction factor from 0 to 0.10 during processing of copper. The effective stress in the tool reaches to ~ 5 GPa during processing of hardened SS, implying an augmentative stress in the rotation roll when processing of high strength materials by CARP at room temperature. The result suggests that tool material selection can be a challenge for processing of high strength materials.

Discussion

Strain distribution

The computed strain distributions during CARP on a Cu sheet as shown in Fig. 3 agree with the earlier reported results for a similar processing technique of SRAR [18, 19, 21] which has similar die design, but has a different extrusion condition during rolling. The present FEM results are in agreement with the theoretical predictions of strain. The total amount of imposed strain $\varepsilon_{\text{total}}$ during processing can be estimated by the sum of the deformation, thus true strain, imposed during the compression of the sheet during rolling ε_{c} , and the strain imposed by shear deformation by ECAP ε_{s} [47], which are given below

$$\varepsilon_{\text{total}} = \varepsilon_{c} + \varepsilon_{s} \\
= \ln\left(\frac{t_{\text{initial}}}{t_{\text{final}}}\right) + \left[\frac{2\cot\left(\frac{\Phi}{2} + \frac{\psi}{2}\right) + \psi \csc\left(\frac{\Phi}{2} + \frac{\psi}{2}\right)}{\sqrt{3}}\right] \tag{2}$$

where t_{initial} is the initial thickness of the sheet of 1.0 mm, $t_{\rm final}$, is the thickness after the compression stage of 0.9 mm, Φ is the angle between the channels in the shear deformation stage of 135°, and ψ is the angle of curvature in the shear deformation zone. The total theoretical strain imposed during deformation should be ~ 0.58 when ψ is considered as 0°. However, processing of materials having strain-hardening ability leads to the formation of a corner gap [28] that in practice increases the value of ψ and decreases the amount of strain imposed [49]. Thus, plastic strains of ~ 0.42 are introduced at the inner surfaces of the copper sheet, while strains of ~ 0.56 are introduced at the outer surfaces of the sheet. The FEM-predicted distribution of strain in this study agrees with the recorded hardness variation across the thickness of the sheet as shown in Fig. 7b, so that the regions with high plastic deformation show an influence of strain hardening.

Capability of metal sheets processing by CARP

It is of great interest to use CARP for processing high strength materials at increased processing speeds, enhancing the efficiency and productivity in sheet metal production. However, material strength, friction, and processing speed affect the generation of heat within the sheet, strength requirements for processing tools, and energy consumption of processing. Considering the processing capability, especially scale-up of CARP for wider sheets, Table 2 summarizes the approximated values through FEM of torque τ , power P, and maximum temperature $T_{\rm max}$ for processing by CARP of a sheet metal with 100 mm width.

The present analysis considers excess heat generation during CARP. The process introduces a large amount of strain in the channel-angle shear deformation zone and most of the work done is expected to be converted into heat. Before discussing the FEM estimation, it is reasonable to evaluate the theoretical calculation of the heat generation through CARP. Equation (3) [56] provides a theoretical calculation of the temperature increase in adiabatic conditions, ΔT , during the metal forming operations by considering the work per volume for plastic deformation ($\sigma \times d\varepsilon$), the fraction of work converted into heat, β , the material density, ρ , and specific heat, c.

$$\Delta T = \frac{\beta \sigma d\varepsilon}{\rho c} \tag{3}$$

The work in CARP can be estimated by the multiplication of the average flow stress and the amount of imposed plastic deformation to the material during the sheet processing operation. The fraction of work converted into heat, β , is usually considered equal to 0.9 [56]. Thus, considering an imposed deformation of 0.5 and average flow stresses of 350, 800 and 1500 MPa, the maximum temperature increases are ~ 45 , ~ 92 and ~ 173 °C for the copper, annealed SS and hardened SS, respectively. However, these values are considered an upper bound on the increase in temperature for each material because the theoretical estimation ignores the dissipation of heat during the processing operation.



The value of T_{max} estimated through present FEM for processing of a copper sheet at 5 mm/s is 24 °C, which reflects an increase of only 4 °C from the initial temperature of 20 °C. Increasing the friction factor to 0.10 produces a minor increase in T_{max} to 7 °C. Although these values are significantly smaller than the predicted by Eq. (3) for copper, a maximum temperature of 50 °C is observed during processing of copper at ~ 53 mm/s because increasing processing velocity reduces the ability of the material to dissipate the heat. Maximum temperatures of ~ 120 °C and ∼ 200 °C are predicted for processing of the annealed and harden stainless steel, respectively, at processing speeds of \sim 53 mm/s. These temperatures agree with the theoretical predictions of Eq. (3), thereby implying that processing of stainless steel at such high velocity produces an adiabatic heating condition. It is important to note that a temperature increase up to 136 °C was reported during ECAP-Conform that introduces an impose strain of ~ 1 in an aluminum alloy at a processing speed of ~ 8.3 mm/s [57]. Although the material and processing conditions differ from the present simulation, the report shows that the pronounced heating can occur during continuous severe plastic deformation processing at high speeds. Such increase in temperature can affect the microstructure development and thus, the mechanical properties.

Another point of concern for scaling up the CARP technique is the requirements of torque that affects tool design and power consumption. The required torque varies slightly with the processing speed since an increase in processing velocity increases the strain rate of the material which increases the flow stress as was shown in Fig. 4 for the copper sheet. However, the material's strength and friction factor play major roles on the torque requirement. There is over a tenfold increase in the estimated torque required when the friction factor is increased from 0 to 0.1 for

the copper sheet. This shows the importance of attaining good surface finishes of the CARP tools and applying lubrication during the process. Also, the torque required to process stainless steel is much higher than for copper. This work shows that the friction factor and material's strength affect the stresses developed in the tools during CARP (Table 3).

Energy incorporated into CARP-processed sheets

It is possible to use the present results to estimate the energy incorporated into a sheet material during CARP. The consumed energy directly affects the cost of sheet processing, and thus the information is of great importance to evaluate the potential of the CARP technique for mass processing of sheet metals. The values of *P* in Table 2 provide the power required for processing the different materials under various friction factors and processing speeds. While the power depends on the torque estimated in the simulations, it follows that friction plays a significant role on the power requirements. The energy incorporated in 1 kg of a material can be estimated by the multiplication of the power and the time required to process the unit mass.

The incorporated energy in copper for a single pass of CARP at 5 mm/s increases from ~ 22 kJ/kg to ~ 130 kJ/kg and ~ 350 kJ/kg with increasing friction factor from 0 to 0.05 and 0.10, respectively. It implies that a large fraction of energy can be spent in friction. The processing velocity has only a minor effect on the incorporated energy. It is important to note that, when additional passes of CARP are required to promote grain refinement, the incorporated energy per pass is expected to increase with increasing the number of passes as the processed material gets work hardened. This is supported by the twofold increase in energy of ~ 330 kJ/kg for the

Table 3 Summary of maximum temperature $T_{\rm max}$, average torque τ , power P, (for a sheet having 100 mm width) and incorporated energy $E_{\rm inc}$, for processing of copper under different friction factor m and velocity v, and stainless steel (SS) in the annealed and hardened conditions

Material	m	$v \text{ (mm s}^{-1}\text{)}$	T _{max} (°C)	τ (kN m)	P (kW)	E_{inc} (kJ kg ⁻¹)
Copper	0.00	5	24	~ 0.85	~ 0.09	~ 22
Copper	0.00	16	32	~ 0.925	~ 0.29	~ 23
Copper	0.00	53	50	~ 0.95	~ 0.99	~ 23
Copper	0.05	5	24	∼ 5.0	~ 0.52	~ 130
Copper	0.10	5	27	~ 13.25	~ 1.4	~ 350
SS (annealed)	0.05	53	118	~ 13.0	~ 13.6	~ 330
SS (hardened)	0.05	53	205	~ 29.5	~ 30.9	~ 740



annealed SS towards ~ 740 kJ/kg for the hardened sample after a single CARP pass. In the current simulation, the incorporated energies in a range of 1–2 MJ/kg are expected for \sim 8 passes of CARP on copper at an intermediate friction factor of 0.05 by considering the hardening of material. The estimated incorporated energy can be even higher for high strength metals including the stainless steel, such as $\sim 5 \,\mathrm{MJ/kg}$ under the similar processing conditions. These values represent a minor fraction of the estimated embodied energy of copper and steel, such as 60-150 MJ/kg for Cu [58] and 77-85 MJ/kg for stainless steel [59], where embodied energy represents the accumulative energy spent from the acquisition of raw materials, their processing and manufacturing, and throughout their service. This suggests that severe plastic deformation processing including CARP does not influence significantly the embodied energy of general engineering metals and materials.

Summary and Conclusions

- FEM was applied to model the SPD technique of CARP. The feasibility of the CARP operation and scaling up the process was evaluated under various processing conditions and parameters including processing speeds and friction factors on copper and stainless steel sheets. Experimental validation is provided for the processing of copper.
- 2. Plastic strains in the range of 0.4–0.6 are imposed in a single pass. Slightly lower values of strain are imposed at the inner sheet surfaces facing to the rotation die, which agrees with the reported strain variations observed after ECAP. The computed strain is in good agreement with the theoretical predictions and are not significantly affected by the material strength, friction, or processing velocity. The distribution of strain is validated by the distribution of hardness measured experimentally, which is influenced by strain hardening of materials.
- The strength of a material being processed affects the torque requirements, heat generation, and stresses developed in the tools. These parameters must be considered for the future development of the CARP technique.

- 4. The increase in friction between a sheet metal and the CARP tools increases significantly the hydrostatic stresses developed within the sheet, the torque required for processing, energy consumption, and the stresses at tools.
- 5. Increasing processing velocity multiply significantly the temperature of the processed material. The maximum temperature increase, during processing at ~ 50 mm/s, reaches near the theoretical prediction for adiabatic heating in metal forming operations.
- 6. The incorporated energies for processing by CARP of sheets for multiple passes were estimated. Values in the range of 1–2 MJ/kg were estimated for copper and ~ 5 MJ/kg for stainless steel. The energy consumed by the severe plastic deformation process is reasonable when considering the embodied energy of the metals.

Acknowledgements

RBF acknowledges financial support from CNPq (Grant #302445/2018-8) and FAPEMIG (Grant TEC-PPM-00324-17). This study for MK and MKS was supported by the National Science Foundation of the United States under Grant No. CMMI-2051205.

Data availability

The datasets generated during and/or analyzed during the current study are available from the corresponding authors on reasonable request.

Declarations

Conflict of Interest The authors declare no conflict of interest.

Ethical approval The authors have adhered to the accepted ethical standards of a genuine research study.

References

[1] Valiev RZ, Estrin Y, Horita Z, Langdon TG, Zehetbauer MJ, Zhu YT (2006) Producing bulk ultrafine-grained materials by severe plastic deformation. JOM 58:33–39. https://doi. org/10.1007/s11837-006-0213-7



- [2] Valiev RZ, Estrin Y, Horita Z, Langdon TG, Zehetbauer MJ, Zhu YT (2016) Producing bulk ultrafine-grained materials by severe plastic deformation: Ten years later. JOM 68:1216–1226. https://doi.org/10.1007/s11837-016-1820-6
- [3] Edalati K, Bachmaier A, Beloshenko VA, Beygelzimer Y, Blank VD, Botta WJ, Bryla K, Cizek J, Divinski S, Enikeev NA, Estrin Y, Faraji G, Figueiredo RB, Fuji M, Furuta T, Grosdidier T, Gubicza J, Hohenwarter A, Horita Z, Huot J, Ikoma Y, Janecek M, Kawasaki M, Kral P, Kuramoto S, Langdon TG, Leiva DR, Levitas VI, Mazilkin A, Mito M, Miyamoto H, Nishizaki T, Pippan R, Popov VV, Popova EN, Purcek G, Renk O, Revesz A, Sauvage X, Sklenicka V, Skrotzki W, Straumal BB, Suwas S, Toth LS, Tsuji N, Valiev RZ, Wilde G, Zehetbauer MJ, Zhu XK (2022) Nanomaterials by severe plastic deformation: review of historical developments and recent advances. Mater Res Lett 10:163–256. https://doi.org/10.1080/21663831.2022.2029779
- [4] Figueiredo RB, Langdon TG (2021) Deformation mechanisms in ultrafine-grained metals with an emphasis on the Hall-Petch relationship and strain rate sensitivity. J Mater Res Technol 14:137–159. https://doi.org/10.1016/j.jmrt.2021.06.016
- [5] Kawasaki M, Langdon TG (2015) Review: achieving superplastic properties in ultrafine-grained materials at high temperatures. J Mater Sci 51:19–32. https://doi.org/10.1007/ s10853-015-9176-9
- [6] V Segal (1977) Materials preparation for following processing, Invention Certificate of USSR. No.575892 Sverdlovsk, Russia,
- [7] VI Kopylov, VM Segal (1977) A device for continuous pressing of metals, Invention Certificate of USSR. No.575151 Sverdlovsk, Russia, .
- [8] Raab GJ, Valiev RZ, Lowe TC, Zhu YT (2004) Continuous processing of ultrafine grained Al by ECAP-conform. Mater Sci Eng A 382:30–34. https://doi.org/10.1016/j.msea.2004. 04.021
- [9] Xu C, Schroeder S, Berbon PB, Langdon TG (2010) Principles of ECAP-Conform as a continuous process for achieving grain refinement: application to an aluminum alloy. Acta Mater 58:1379–1386. https://doi.org/10.1016/j.actamat.2009.10.044
- [10] Raab GI, Valiev R, Gunderov D, Lowe TC, Misra A (2008) YT Zhu Long-length ultrafine-grained titanium rods produced by ECAP-conform. Mater Sci Forum 584–586:80–85. https://doi.org/10.4028/www.scientific.net/MSF.584-586.80
- [11] Lowe TC, Valiev RZ, Li XC, Ewing BR (2021) Commercialization of bulk nanostructured metals and alloys. MRS Bull 46:265–272. https://doi.org/10.1557/s43577-021-0006 0-0

- [12] Azimi A, Tutunchilar S, Faraji G, Givi MKB (2012) Mechanical properties and microstructural evolution during multi-pass ECAR of Al 1100-O alloy. Mater Design 42:388–394. https://doi.org/10.1016/j.matdes.2012.06.035
- [13] Chung YH, Park JW, Lee KH (2006) An analysis of accumulated deformation in the equal channel angular rolling (ECAR) process. Met Mater Int 12:289–292. https://doi.org/ 10.1007/Bf03027545
- [14] Honarpisheh M, Entezami SS, Akhavan S (2019) Effect of equal channel angular rolling process on the fracture mechanisms of Al-7057 and Al-5052 alloys. Metallogr Microstruct Anal 8:336–348. https://doi.org/10.1007/s13632-019-00540-5
- [15] Cheng YQ, Chen ZH, Xia WJ (2007) Drawability of AZ31 magnesium alloy sheet produced by equal channel angular rolling at room temperature. Mater Charact 58:617–622. h ttps://doi.org/10.1016/j.matchar.2006.07.007
- [16] Habibi A, Ketabchi M, Eskandarzadeh M (2011) Nano-grained pure copper with high-strength and high-conductivity produced by equal channel angular rolling process. J Mater Process Tech 211:1085–1090. https://doi.org/10.1016/j.jmatprotec.2011.01.009
- [17] Huang Y, Prangnell PB (2007) Continuous frictional angular extrusion and its application in the production of ultrafine-grained sheet metals. Scripta Mater 56:333–336. https://doi.org/10.1016/j.scriptamat.2006.11.011
- [18] Lee HH, Yoon JI, Kim HS (2018) Single-roll angular-rolling: A new continuous severe plastic deformation process for metal sheets. Scripta Mater 146:204–207. https://doi.org/10. 1016/j.scriptamat.2017.11.043
- [19] Lee HH, Yoon JI, Park HK, Kim HS (2019) Unique microstructure and simultaneous enhancements of strength and ductility in gradient-microstructured Cu sheet produced by single-roll angular-rolling. Acta Mater 166:638–649. h ttps://doi.org/10.1016/j.actamat.2019.01.021
- [20] Lee HH, Park HK, Jung J, Hwang KJ, Kim HS (2019) Microstructural tailoring in reverse gradient-structured copper sheet using single-roll angular-rolling and subsequent annealing. Mater Sci Eng A 764:138258. https://doi.org/10. 1016/j.msea.2019.138258
- [21] Lee HH, Hwang KJ, Park HK, Kim HS (2020) Effect of processing route on microstructure and mechanical properties in single-roll angular-rolling. Materials 13:2471. http s://doi.org/10.3390/ma13112471
- [22] Lee HH, Park HK, Jung J, Amanov A, Kim HS (2020) Multi-layered gradient structure manufactured by single-roll angular-rolling and ultrasonic nanocrystalline surface modification. Scripta Mater 186:52–56. https://doi.org/10.1016/j. scriptamat.2020.03.051



- [23] Pereira PHR, Figueiredo RB (2019) Finite element modelling of high-pressure torsion: an overview. Mater Trans 60:1139–1150. https://doi.org/10.2320/matertrans. MF201906
- [24] Hu JM, Kulagin R, Ivanisenko Y, Baretzky B, Zhang H (2020) Finite element modeling of Conform-HPTE process for a continuous severe plastic deformation path. J Manuf Process 55:373–380. https://doi.org/10.1016/j.jmapro.2020. 04.052
- [25] Kocich R, Kuncicka L, Mihola M, Skotnicova K (2013) Numerical and experimental analysis of twist channel angular pressing (TCAP) as a SPD process. Mater Sci Eng A 563:86–94. https://doi.org/10.1016/j.msea.2012.11.047
- [26] Prangnell PB, Harris C, Roberts SM (1997) Finite element modelling of equal channel angular extrusion. Scripta Mater 37:983–989. https://doi.org/10.1016/S1359-6462(97)00192-9
- [27] Bowen JR, Gholinia A, Roberts SM, Prangnell PB (2000) Analysis of the billet deformation behaviour in equal channel angular extrusion. Mater Sci Eng A 287:87–99. https://doi. org/10.1016/S0921-5093(00)00834-0
- [28] Kim HS, Seo MH, Hong SI (2000) On the die corner gap formation in equal channel angular pressing. Mater Sci Eng A 291:86–90. https://doi.org/10.1016/S0921-5093(00)0097 0-9
- [29] Li S, Bourke MAM, Beyerlein IJ, Alexander DJ, Clausen B (2004) Finite element analysis of the plastic deformation zone and working load in equal channel angular extrusion. Mater Sci Eng A 382:217–236. https://doi.org/10.1016/j.ms ea.2004.04.067
- [30] DeLo DP, Semiatin SL (1999) Finite-element modeling of nonisothermal equal-channel angular extrusion. Metall Mater Trans A 30:1391–1402. https://doi.org/10.1007/s116 61-999-0287-2
- [31] Semiatin SL, Delo DP, Shell EB (2000) The effect of material properties and tooling design on deformation and fracture during equal channel angular extrusion. Acta Mater 48:1841–1851. https://doi.org/10.1016/S1359-6454(00)000 19-7
- [32] Figueiredo RB, Cetlin PR, Langdon TG (2007) The processing of difficult-to-work alloys by ECAP with an emphasis on magnesium alloys. Acta Mater 55:4769–4779. https://doi.org/10.1016/j.actamat.2007.04.043
- [33] Figueiredo RB, Cetlin PR, Langdon TG (2009) The evolution of damage in perfect-plastic and strain hardening materials processed by equal-channel angular pressing. Mater Sci Eng A 518:124–131. https://doi.org/10.1016/j.msea.2009.04.007
- [34] Cetlin PR, Aguilar MTP, Figueiredo RB, Langdon TG (2010) Avoiding cracks and inhomogeneities in billets

- processed by ECAP. J Mater Sci 45:4561–4570. https://doi.org/10.1007/s10853-010-4384-9
- [35] Figueiredo RB, Aguilar MTP, Cetlin PR (2006) Finite element modelling of plastic instability during ECAP processing of flow-softening materials. Mater Sci Eng A 430:179–184. https://doi.org/10.1016/j.msea.2006.05.116
- [36] Figueiredo RB, Cetlin PR, Langdon TG (2009) Stable and unstable flow in materials processed by equal-channel angular pressing with an emphasis on magnesium alloys. Metall Mater Trans A 41A:778–786. https://doi.org/10.1007/ s11661-009-0100-2
- [37] Lapovok RYE (2005) The role of back-pressure in equal channel angular extrusion. J Mater Sci 40:341–346. https://d oi.org/10.1007/s10853-005-6088-0
- [38] Xu SB, Zhao GQ, Ren W, Guan YJ (2008) Numerical investigation of aluminum deformation behavior in threedimensional continuous confined strip shearing process. Mater Sci Eng A 476:281–289. https://doi.org/10.1016/j.ms ea.2007.05.003
- [39] Wei W, Zhang W, Wei KX, Zhong Y, Cheng G, Hu J (2009) Finite element analysis of deformation behavior in continuous ECAP process. Mater Sci Eng A 516:111–118. https://doi.org/10.1016/j.msea.2009.03.001
- [40] Gholami J, Sedighi M, Pourbashiri M (2015) Effect of channel angle and friction in modified ECAP-Conform process of Al-6061: a numerical study. Iran J Mater Sci Eng 12:71–76. https://doi.org/10.22068/ijmse.12.4.71
- [41] Nemati Chari R, Mollaei Dariani B, Fallahi Arezodar A (2016) Numerical and experimental studies on deformation behavior of 5083 aluminum alloy strips in equal channel angular rolling. Proc Inst Mech Eng B J Eng Manuf 232:1031–1043. https://doi.org/10.1177/0954405416661005
- [42] QForm 10.1.3 [program]. https://www.qform3d.com/
- [43] Levanov AN (1997) Improvement of metal forming processes by means of useful effects of plastic friction. J Mater Process Tech 72:314–316. https://doi.org/10.1016/S0924-01 36(97)00191-X
- [44] Alawadhi MY, Sabbaghianrad S, Huang Y, Langdon TG (2017) Direct influence of recovery behaviour on mechanical properties in oxygen-free copper processed using different SPD techniques: HPT and ECAP. J Mater Res Technol 6:369–377. https://doi.org/10.1016/j.jmrt.2017.05.005
- [45] Huang Y, Sabbaghianrad S, Almazrouee AI, Al-Fadhalah KJ, Alhajeri SN, Langdon TG (2016) The significance of self-annealing at room temperature in high purity copper processed by high-pressure torsion. Mater Sci Eng A 656:55–66. https://doi.org/10.1016/j.msea.2016.01.027
- [46] Alawadhi MY, Sabbaghianrad S, Huang Y, Langdon TG (2020) The stability of oxygen-free copper processed by high-pressure torsion after room temperature storage for



- 12 months. Adv Eng Mater 22:1901015. https://doi.org/10.1002/adem.201901015
- [47] Iwahashi Y, Wang JT, Horita Z, Nemoto M, Langdon TG (1996) Principle of equal-channel angular pressing for the processing of ultra-fine grained materials. Scripta Mater 35:143–146. https://doi.org/10.1016/1359-6462(96)00107-8
- [48] Alateyah AI, Ahmed MMZ, Zedan Y, Abd El-Hafez H, Alawad MO, El-Garaihy WH (2021) Experimental and numerical investigation of the ECAP processed copper: microstructural evolution crystallographic texture and hardness homogeneity. Metals 11:607. https://doi.org/10.3390/ met11040607
- [49] Nakashima K, Horita Z, Nemoto M, Langdon TG (2000) Development of a multi-pass facility for equal-channel angular pressing to high total strains. Mater Sci Eng A 281:82–87. https://doi.org/10.1016/S0921-5093(99)00744-3
- [50] Atefi S, Parsa MH, Ahmadkhaniha D, Zanella C, Jafarian HR (2022) A study on microstructure development and mechanical properties of pure copper subjected to severe plastic deformation by the ECAP-Conform process. J Mater Res Tech 21:1614–1629. https://doi.org/10.1016/j.jmrt.2022.09.103
- [51] Hohenwarter A (2015) Incremental high pressure torsion as a novel severe plastic deformation process: Processing features and application to copper. Mater Sci Eng A 626:80–85. h ttps://doi.org/10.1016/j.msea.2014.12.041
- [52] Edalati K, Horita Z (2010) Continuous high-pressure torsion. J Mater Sci 45:4578–4582. https://doi.org/10.1007/s10853-010-4381-z
- [53] Edalati K, Lee S, Horita Z (2012) Continuous high-pressure torsion using wires. J Mater Sci 47:473–478. https://doi.org/ 10.1007/s10853-011-5822-z
- [54] Leo P, Cerri E, De Marco PP, Roven HJ (2007) Properties and deformation behaviour of severe plastic deformed

- aluminium alloys. J Mater Process Tech 182:207–214. https://doi.org/10.1016/j.jmatprotec.2006.07.038
- [55] Sordi VL, Mendes Filho AA, Valio GT, Springer P, Rubert JB, Ferrante M (2015) Equal-channel angular pressing: influence of die design on pressure forces, strain homogeneity and corner gap formation. J Mater Sci 51:2380–2393. https://doi.org/10.1007/s10853-015-9547-2
- [56] Meyers MA, Xu YB, Xue Q, Perez-Prado MT, McNelley TR (2003) Microstructural evolution in adiabatic shear localization in stainless steel. Acta Mater 51:1307–1325. https://d oi.org/10.1016/S1359-6454(02)00526-8
- [57] Kubina T, Kövér M, Dlouhý J, Nacházel J (2015) Link between technological parameters and material properties of EN 6082 Processed by ECAP-CONFORM and precipitation hardening. Int J Mater Mech Eng 4:36–43. https://doi.org/10. 14355/IJMME.2015.04.006
- [58] Allwood JM, Ashby MF, Gutowski TG, Worrell E (2011) Material efficiency: a white paper. Resour Conserv Recy 55:362–381. https://doi.org/10.1016/j.resconrec.2010.11.002
- [59] Ahmad N, Enemuoh EU (2020) Energy modeling and eco impact evaluation in direct metal laser sintering hybrid milling. Heliyon 6:e03168. https://doi.org/10.1016/j.heliyon. 2020.e03168

Publisher's Note Springer Nature remains neutral with regard to jurisdictional claims in published maps and institutional affiliations.

Springer Nature or its licensor (e.g. a society or other partner) holds exclusive rights to this article under a publishing agreement with the author(s) or other rightsholder(s); author self-archiving of the accepted manuscript version of this article is solely governed by the terms of such publishing agreement and applicable law.

